Supplemental Materials
Network Discovery

Participants

Participants at the Boston and Pittsburgh sites were recruited for a clinical trial (BICEPS, NCT01561859), approved by the institutional review boards of the University of Pittsburg and Beth Israel Deaconess Medical Center, and gave written informed consent before participating. Clinical and imaging data analyzed here was from participants' baseline (pre-intervention) evaluation. Participants were recruited from participating health centers using a variety of means including early course treatment programs and community referral networks

Diagnosis was determined using the Structured Clinical Interview for the DSM-IV (SCID)(1). Patients were assessed by trained research assistant or graduate students. All participants in the schizophrenia group met DSM-IVTR criteria for the diagnosis of schizophrenia or schizoaffective disorder. Inclusion criteria were (1) a diagnosis of schizophrenia or schizoaffective disorder verified using the SCID interview(1); (2) time since first psychotic symptom of $\leq$ 8 years; (3) clinically stabilized on antipsychotic medication (assessed via SCID in consensus conferences); (4) age 18-45 years; (5) current IQ $\geq$ 80; and (6) the ability to read (sixth grade level or higher) and speak fluent English. Exclusion criteria were (1) significant neurological or medical disorders that may produce cognitive impairment (e.g., seizure disorder, traumatic brain injury); (2) persistent suicidal or homicidal behavior; (3) a recent history of substance abuse or dependence (within the past 3 months); (4) any MRI contraindications such as ferromagnetic objects in the body and those people too large to fit into the scanner (shoulder width larger than 25 inches); and (5) decisional incapacity requiring a

guardian. Participant clinical characterization utilized symptom scales including the Scale for the Assessment of Positive Symptoms (SAPS)(2), Scale for the Assessment of Negative Symptoms (SANS)(3), the Brief Psychiatric Rating Scale (BPRS)(4), and the Montgomery–Åsberg Depression Rating Scale (MADRS)(5). Demographic, clinical, and medication regimen information are summarized in Table 1.

MRI data acquisition

Boston Site: Data were acquired on a 3T Siemens Trio (TIM upgrade) scanner using a standard head coil. The echoplanar imaging parameters were as follows: repetition time, 3000 milliseconds; echo time, 30 milliseconds; flip angle, 85°; 3 x 3 x 3-mm voxels; and 47 axial sections collected with interleaved acquisition and no gap. Structural data included a $1mm^3$ multiecho, T1-weighted, magnetization-prepared, gradient-echo image. In addition, all participants underwent a resting fMRI run. Each functional run lasted 6.2 minutes (124 time points).

Pittsburgh site: Data were acquired on a 3T Siemens Verio scanner using a standard head coil. The echoplanar imaging parameters were as follows: repetition time, 3000 milliseconds; echo time, 30 milliseconds; flip angle, 85°; 3 x 3 x 3-mm voxels; and 45 axial sections collected with interleaved acquisition and no gap. Structural data included a $1mm^3$ multiecho, T1-weighted, magnetization-prepared, gradient-echo image. In addition, all participants underwent a resting fMRI run. Each functional run lasted 6.2 minutes (124 time points).

MRI data processing

The imaging data were preprocessed using DPABI image processing software (6). To minimize effects of scanner signal stabilization, the first four images were

omitted from all analysis. Scans with head motion exceeding 3mm or 3^0 of maximum rotation through the resting-state run were discarded. Functional and structural images were co-registered. Structural images were then normalized and segmented into gray, white and CSF partitions using the DARTEL technique. A Friston 24-parameter model was used to regress out head motion effects from the realigned data. CSF, white matter, and the global signals as well as the linear trend were also regressed as nuisance covariates. After realigning, slice timing correction, and co-registration, framewise displacement (FD) was calculated for all resting state volumes (7). All volumes with a FD greater than 0.2mm were regressed out as nuisance covariates. Any scan with 50% of volumes removed was discarded. After nuisance covariate regression, the resultant data were band pass filtered to select low frequency (0.01-0.08Hz) signals. Filtered data were normalized by DARTEL into MNI space and then smoothed by a Gaussian kernel of $8mm^3$ full-width at half maximum (FWHM). Voxels within a group derived gray matter mask were used for further analyses.

After preprocessing, 36 scans were rejected for excessive motion. A total of 44 participants with schizophrenia or schizoaffective disorder remained in the study (Table 1).

Functional Connectivity Analysis:

Multivariate Distance Matrix Regression: We performed a connectome-wide association study using multivariate distance matrix regression (MDMR) as originally described in Shehzad et al.(8). As has been previously described(9-11) this analysis occurs in three stages: First, a seed-to-voxel connectivity map is generated by using an individual voxel's BOLD signal time-course to calculate the temporal Pearson's

correlation coefficients between that voxel and all other gray matter voxels. These maps are generated for every participant. In the second stage, the correlation coefficients for each voxel in the connectivity map is compared to the values of corresponding voxels in maps generated from every other participant. This results in a Pearson's correlation coefficient *r* that is a measure of spatial correlation of maps between patients. The similarity of connectivity maps between participants is computed using the distance metric $\sqrt{2(1-r)}$. In the third stage, multivariate distance matrix regression tests the relationship between inter-subject differences on a given variable (here SANS score) and inter-subject distances on the connectivity maps generated in stage two (See main text Figure 1a for a diagram of this process). This test results in a pseudo-F statistic for each voxel that demonstrates how SANS score is reflected in functional connectivity at that voxel. This process is repeated for every single voxel. The result is a whole brain map of how significantly SANS score is reflected in functional connectivity at every voxel. Covariates included in this analysis included scanner site, age, sex, mean FD (as a subject-level correction for motion effects(7)), and prescribed antipsychotic dosage (chlorpromazine equivalents, CPZE). To correct for multiple comparisons, a nonparametric permutation was calculated for voxels that exceeded the significance threshold of $p < 0.005$ and clusters of such of sizes at a threshold of $p < 0.05$ (12), with a null distribution calculated from 5000 such permutations, as in prior MDMR studies.

This analysis identifies regions of interest (ROI) where SANS score correlates with functional connectivity. The steps of the analysis described above do not display the pattern or direction (i.e. correlation vs anti-correlation) of connectivity that generated the result. To visualize these patterns, it is necessary to conduct post-hoc testing of the

regions of interest identified from MDMR. This ROI-based analysis allows visualization of the connectivity maps that generated the initial result. As others have emphasized (9-11), these post-hoc tests are not new hypothesis tests, rather, they allow visualization of the connectivity that gave rise to the original MDMR result.

ROI based analyses

For ROI based analyses we used DPABI to extract the time course of the BOLD signal in a given ROI and then generated whole brain maps of z-transformed Pearson's correlation coefficients. These maps were then entered into SPM12 (Statistical and Parametric Mapping, http://www.fil.ion.ucl.ac.uk/spm). For the right dorsolateral prefrontal cortex ROI generated from MDMR above, we regressed these maps against total SANS score to generate maps of how whole brain functional connectivity to the ROIs varies with SANS score. As in the MDMR analyses, SPM analyses included site, sex, age, mean FD, and prescribed antipsychotic dosage as covariates.

Network Validation

Participants

Data for the network validation study was taken from a registered clinical trial for cerebellar TMS (NCT01551979), which was approved by the Institutional Review Board of Beth Israel Deaconess Medical Center, and all participants gave written informed consent before participating. Participants were recruited from participating health centers using a variety of means including recruitment from previous experimental participation rosters, flyers, and websites including clinicaltrials.gov.

Diagnosis was determined by psychiatrist evaluation and medical records review. All participants were diagnosed with schizophrenia. Eligible subjects were 18-65 years of

age. For the month before enrollment they received outpatient care, with no hospitalizations, and without changes to their medication regimens. Exclusion criteria were substance abuse or dependence in the prior six months, a history of seizures, head injury or prior neurosurgical procedures, contraindications to TMS or MRI, gross organic pathology on neuroimaging, and pregnancy in females.

Participant clinical characterization included Positive and Negative Syndrome Scale (PANSS)(13), Calgary Depression Scale for Schizophrenia(14), and Clinical Global Impression (CGI)

Clinician administered symptom scales were collected at baseline, on day 5 of rTMS, and one week after day 5 of rTMS (the same day as imaging). 22 total participants were enrolled in the study, of which 17 participants were randomized, 16 completed the trial to the point of followup, and data from 11 participants passed quality control assessments (See consort Figure)

Demographic, clinical, and medication regimen information are summarized in Table 1.

MRI data acquisition

Boston Site: Data were acquired on a 3T Siemens Tim Trio scanner using a standard head coil. The echoplanar imaging parameters were as follows: repetition time, 3000 milliseconds; echo time, 30 milliseconds; flip angle, 90°; 3 x 3 x 3-mm voxels; and 47 axial sections collected with interleaved acquisition and no gap. A $1mm^3$ multi-echo MPRAGE was also collected. In addition, all participants underwent three resting state fMRI runs. Each functional run lasted 6 minutes (124 time points), with 4 time points used for steady state equilibrium. Participants completed a minimum of three resting state functional runs. The imaging protocol was adapted from the previous

acute stimulation protocol(15). MRI imaging occurred at baseline and one week after day 5 of rTMS, with a +/-3 day allowance for scheduling.

MRI data processing

The imaging data were preprocessed using DPABI image processing software (6). To minimize effects of scanner signal stabilization, the first four images were omitted from all analysis. Scans with head motion exceeding 3 mm or 3° of maximum rotation through the resting-state run were discarded. Functional and structural images were co-registered. Structural images were then normalized and segmented into gray, white and CSF partitions using the DARTEL technique. A Friston 24-parameter model was used to regress out head motion effects from the realigned data. CSF and white matter signals as well as the linear trend were also regressed as nuisance covariates. After realigning, slice timing correction, and co-registration, framewise displacement (FD) was calculated for all resting state volumes (7). All volumes with a FD greater than 0.5mm were regressed out as nuisance covariates. Any scan with 50% of volumes removed was discarded. After nuisance covariate regression, the resultant data were band pass filtered to select low frequency (0.01-0.08Hz) signals. Filtered data were normalized by DARTEL into MNI space and then smoothed by a Gaussian kernel of $8mm^3$ full-width at half maximum (FWHM). Voxels within a group derived gray matter mask were used for further analyses.

After preprocessing, 11 participants had clinical assessment and usable fMRI scan data at both baseline and one week post-rTMS. 4 participants did not have usable fMRI information at one or both time points after exclusion for in-scanner motion (see consort).

rTMS protocol:

Theta-burst stimulation of the cerebellum was performed as before(16) Baseline anatomical MRIs were used in Brainsight frameless stereotaxic system (Rogue Research, Montreal, Canada) to target anatomically determined cerebellar vermis VIIB. Frameless sterotaxy was used during all stimulation sessions to monitor the position of coil over the duration of theta-burst. Participants received 10 sessions of either TBS or sham stimulation to the cerebellar vermis. Participants were seated in a chair with their head facing downwards. TBS sessions were administered twice daily separated by a minimum of 4 hours on five consecutive days, Monday to Friday. Participants were either admitted to the BIDMC clinical research center unit for the week and waited in their room, or if participants opted to participate as out-patients, were given a quiet room to rest in-between daily sessions. TBS was applied via a MagPro X100 stimulator using a combination active and passive figure-of-8 coil (Cool B65 A/P, Magventure, Denmark) held tangentially to the scalp with the handle pointing upwards. Shamming surface electrodes were placed on all participants at the neck-line to simulate the tactile effects of stimulation. Stimulation codes were used by the TBS was applied at 100% of active motor threshold (AMT) intensity (A/μs) measured prior to each theta-burst session with the standard intermittent theta burst pattern described by Huang et al.(17) (3 pulses at 50-Hz repeated at a rate of 5-Hz).

Imaging Data Analysis

For the initial ROI to ROI based analysis we took the map (thresholded at T-stat > 2.0 i.e. $p<.05$) from the “network identification” study of where functional connectivity

to the right dorsolateral prefrontal cortex correlated with SANS score. Masks of the right dorsolateral prefrontal cortex and cerebellar ROIs were used for the analysis of pre- vs post-rTMS fMRI data from study #2. We used DPABI to calculate the time course of the BOLD signal in each ROI and then generated z-transformed Pearson's correlation coefficients for each resting-state run for each participant at each time point. For each participant we calculated the change in functional connectivity pre- versus post-rTMS and correlated this change with that individual's change in PANSS negative symptom subscale between baseline assessment and one week post-rTMS when fMRI imaging occurred.

For the second ROI to voxel based analysis, we took the right dorsolateral prefrontal cortex ROI from the "network identification" study as above. We used DPABI to calculate the time course of the BOLD signal in this ROI and then generated whole brain maps of z-transformed Pearson's correlation coefficients for each participant. Pre-rTMS maps were subtracted from post-rTMS maps to generate maps of functional connectivity change for each participant. These maps were then entered into SPM12 (Statistical and Parametric Mapping, http://www.fil.ion.ucl.ac.uk/spm). We regressed these maps against each individual's change in total PANSS negative subscore (pre- versus post-rTMS) to generate maps of how change in whole brain functional connectivity to the right dorsolateral prefrontal cortex varies with change in PANSS negative subscore.

Sham vs. active rTMS comparison

Of the 11 participants with full clinical assessments and usable fMRI scan data at baseline and one week post-rTMS, 8 had been randomized to active stimulation and 3 to the sham condition. A Welch's t-test was used to compare change in zFC (between R dorsolateral prefrontal cortex and the cerebellum territory identified above) and change in PANSS negative subscore between groups (active v. sham).

TMS protocol adverse events

A number of expected adverse events occurred during the TMS trial. Four participants reported headache over the course of the trial. Three participants reported neck pain. One participant reported "pressure" on the scalp over the ears and top of the scalp. One participant reported a heaviness on the right side of the head during and after the first three days of TMS. One participant reported feeling tired following two of the TMS sessions. A blood pressure increase was reported on one participant following TMS. One participant reported feeling depressed during the followup period (>3 weeks post-TMS). One participant was hospitalized during the followup period ((>3 weeks post-TMS) for acute exacerbation of psychosis.

Control Analysis

Left dorsolateral prefrontal cortex (MDMR identified)

MDMR identified two different clusters in prefrontal cortex, but gave a larger pseudo-F statistic for right dorsolateral prefrontal cortex compared to the left dorsolateral prefrontal cortex. A similar post-hoc analysis was done from left dorsolateral prefrontal

cortex in the network identification cohort and revealed largely similar network negative symptom network organization, Supplemental Figure 1. Using the same cerebellar region of interest as in main text, but examining functional connectivity to left dorsolateral prefrontal cortex reveals similar functional connectivity values as the cerebellum to right dorsolateral prefrontal cortex (r= 0.71; p=0.014; %95 CI: 0.192, 0.918).

Cerebellum

The main text contains an analysis utilizing the right dorsolateral prefrontal cortex site identified with MDMR and observing the change in connectivity (to right dorsolateral prefrontal cortex) that corresponds to negative symptom change in the validation TMS experiment. This analysis confirmed that only the cerebellum showed functional connectivity change (Figure 3). To confirm the changes in functional connectivity were primarily observed in right dorosolateral prefrontal cortex, we performed a follow-up analysis, seeding the cerebellum and observing the voxelwise change in connectivity that corresponds to symptom severity. A peak cluster (center of gravity MNI: 41.8, 19.9, 40.7) was observed at the same right dorsolateral prefrontal cortex location that the initial discovery dataset indicated shown in Supplemental Figure 2.

Non-parametric statistics.

With a low sample size, it is potentially possible that Pearson correlation coefficients may not remain robust. Thus, we applied a non-parametric test of relationship between the change in functional connectivity between cerebellum and dorsolateral prefrontal

cortex and the change in negative symptoms with Spearman's rho (ρ=-0.741, p=0.0102, bootstrapped 95% CI: -0.970, -0.184), which revealed no change in hypothesis outcome compared to a Pearson correlation coefficient (r=-0.809, p=0.003, 95% CI: -0.948, -0.405).

Positive and General PANSS sub-scales

The main text contains an analysis associating observed changes in cerebellar-dorsolateral prefrontal cortex locations with observed changes in negative symptoms. These changes appear isolated to the PANSS-negative subscale. Connectivity change does not correspond with PANSS-positive subscale (r=0.253; p=0.453; 95% CI: -0.408, 0.74) or with PANSS-general subscale (r=-0.494; p=0.123; 95% CI: -0.843, 0.15). The connectivity change also did not correspond to change in the Calgary Depression Scale for Schizophrenia (r=-.434; p=.183; 95% CI: -0.82, 0.224)

Clozapine equivalent dose

Our primary analysis of change scores in the validation cohort did not control for medication dosage. Controlling for medication effect in a pre-post design is less informative than in a cross-sectional study where medication may co-vary by participant. In a pre-post experimental design, variance attributed to medication may already be removed by examining the difference scores. However, there may exist an interaction, such that medication dose effects many differentially impact the magnitude of changes observed. To control for this, we performed a partial correlation, controlling for Clozapine equivalent doses in the participants (r=-0.817, p=0.004), and found no

change in statistical outcome in comparison to the uncontrolled analysis in the main text (r=-0.809, p=0.003)

Historical evidence for a cerebellar – prefrontal circuit in negative symptoms

There exist two long-standing independent hypotheses that cerebellar and lateral prefrontal regions are associated with symptoms of schizophrenia. Even the earliest descriptions of dementia praecox by Kraepelin specify a frontal cortex origin of the disease(18). With the advent of neuroimaging techniques, frontal circuit abnormalities were often found in schizophrenia patients relative to controls (19, 20), and in task-based studies, these deficits were larger in patients with negative symptoms (21). Modern understanding of a potential cerebellar origin to negative symptoms of schizophrenia was put forward by Schmahmann (22, 23) and subsequently followed by preliminary imaging results from Andreasen and colleagues (24). The foundation of the cerebellar hypothesis is schizophrenia is a form of dysmetria in a cognitive domain – that the same characteristic undercorrection and overcorrection of a motor movement caused by cerebellar damage to motor systems, may be translated in to the responses of schizophrenia patients in the cognitive and emotional domains. This theory was termed “dysmetria of thought.” Despite consistent neuroimaging findings in frontal cortex and in the cerebellum over the years(25-27), the frontal component of this system has been at the forefront of neuroimaging findings, and the cerebellar component is often ignored, recent reviews of the disease do not consider these hypotheses(28). Although cerebellar neuroimaging findings are consistent with a dysmetria of thought model, it still remains uncertain if these results are due to the

fundamental linkage of connectivity between the cerebellum and cortex, and thus are seen active when cortical function is active, (or dysfunctional)(29). It may be plausible that a subset of schizophrenia symptoms may be attributable to this cerebellar-cortical circuity, whereas others are attributed to other dysfunction found throughout the brain. The specific framework of the dysmetria of thought hypothesis has not elucidated a candidate network location. We speculate that cerebellar dysfunction may be present throughout the entire cerebellum, which may account for the broad spectrum of tasks which show cerebellar deficits (25). Many of these studies have examined patients as a population relative to controls. However, our model-free data point to a more localized region within the cerebellum where disruption of connectivity coincides with symptom severity, suggesting that specific connections may account for specific features of a heterogenous illness such as schizophrenia.

Supplemental Table 1: MRI scan parameters across sites/study

Anatomical

	Network Discovery (Boston / Martinos)	**Network Discovery (Pittsburg / SIBR)**	**Network Validation (Boston / Harvard)**
Scanner model	TrioTim	Verio	TrioTim
Software Version	syngo MR B17	syngo MR B17	syngo MR B17
Sequence	MPRAGE	MPRAGE	multiecho MPRAGE
Echo Time (TE)	3.44	3.47	1.64
Inversion Time (TI)	1100	1100	1200
Repetition Time (TR)	2530	2530	2200
Flip Angle	7	7	7
Voxel size	1 mm^3	1 mm^3	1 mm^3

Functional resting state

	Network Discovery (Boston / Martinos)	**Network Discovery (Pittsburg / SIBR)**	**Network Validation (Boston / Harvard)**
Scanner model	TrioTim	Verio	TrioTim
Software Version	syngo MR B17	syngo MR B17	syngo MR B17
Flip angle	85	85	90
Echo Time (TE)	30	30	30
Repetition Time (TR)	3000	3000	3000
Voxel size	3 mm^3	3 mm^3	3 mm^3
Slice Order	interleaved	interleaved	interleaved
Number of TRs / scan	124	124	124

Supplemental Table 2: Cluster locations from post-hoc analysis

clusters with positive relationship with SANS to functional connectivity from R DLPFC

p(FDR-corr)	Size	peak locations			
		T	x	y	z
0	4019	5.25	27	-42	48
		5.15	-3	-81	39
		4.65	-9	-78	24
0.007	746	3.89	21	3	63
		3.78	30	0	54
		3.44	42	-6	51

clusters with negative relationship with SANS to functional connectivity from R DLPFC

p(FDR-corr)	Size	peak locations			
		T	x	y	z
0.003	869	5.14	-9	-96	-27
		3.79	42	-66	-39
		3.7	-15	-75	-24
0.025	434	4.52	60	-12	-24
		4.23	57	-18	-15
		3.93	69	-18	-3
0.014	527	4.52	-51	-66	30
		4.4	-51	-66	39
		3.33	-63	-51	21
0	1557	4.46	-12	30	45
		4.23	-15	60	36
		3.86	15	33	45
0.028	405	4.05	51	-63	51
		3.61	39	-60	36
0.005	733	4.04	-57	-42	-9
		3.75	-42	-27	-9
		3.65	-54	-18	-18
0.009	614	3.88	6	-57	42
		3.84	-3	-63	42
		3.81	0	-48	21

clusters with positive relationship with SANS to functional connectivity from L DLPFC

p(FDR-corr)	Size	peak locations			
		T	x	y	z
0	3699	5.37	6	24	24

		5.27	6	-54	66
		5.26	-6	24	21
0.009	756	4.12	-36	12	-3
		4.1	-42	9	3
		3.96	-36	12	9
0.026	565	3.59	36	15	-6
		3.47	42	21	-3
		2.93	63	-6	3

clusters with negative relationship with SANS to functional connectivity from L DLPFC

p(FDR-corr)	**Size**	**peak locations**			
		T	**x**	**y**	**z**
0.001	1260	5.31	-39	21	45
		4.39	15	33	42
		4.15	36	21	51
0.022	568	4.96	39	-57	45
		4.87	48	-60	45
		2.49	54	-63	24
0.052	363	4.67	15	-63	-39
		3.33	33	-72	-39
		3.32	15	-93	-30
0.04	431	4.66	6	-30	33
		3.56	-15	-39	33
		2.9	6	-45	27
0.046	395	4.48	60	-15	-24
		3.83	66	-27	-6
		3.8	54	-39	-15
0.029	498	3.97	-33	-60	51
		3.51	-48	-69	45
		3.14	-51	-66	27
0.022	618	3.83	18	30	-15
		3.62	36	36	-18
		3.17	45	57	9

Supplemental Table 3. PANSS and cerebellar-dorsolateral prefrontal cortex functional connectivity values for individual participants.

		PANSS (baseline)			PANSS (post TMS)			FC CB-DLPFC [z(r)]		PANSS (change)			FC
ID	Group	pos	neg	gen	pos	neg	gen	baseline	post	pos	neg	gen	change
S001	sham	14	19	39	11	18	28	-0.063555	-0.283037	-3	-1	-11	-0.219482
S002	real	15	16	23	10	12	19	0.290845	0.301866	-5	-4	-4	0.01102
S003	sham	7	33	41	7	33	41	0.248199	-0.006861	0	0	0	-0.25506
S004	sham	16	13	20	14	12	22	0.19712	0.081041	-2	-1	2	-0.116079
S005	real	29	12	34	17	12	31	-0.054101	-0.311363	-12	0	-3	-0.257261
S006	real	12	22	35	10	19	31	0.116081	0.142335	-2	-3	-4	0.026255
S007	real	16	26	29	13	18	22	-0.475664	-0.001296	-3	-8	-7	0.474368
S008	real	19	35	40	12	31	26	-0.405339	-0.261537	-7	-4	-14	0.143802
S009	real	18	30	52	8	21	32	-0.099842	0.181747	-10	-9	-20	0.281589
S010	real	24	40	57	18	34	46	0.231574	0.401537	-6	-6	-11	0.169963
S011	real	18	7	24	13	7	19	-0.021016	-0.217381	-5	0	-5	-0.196365

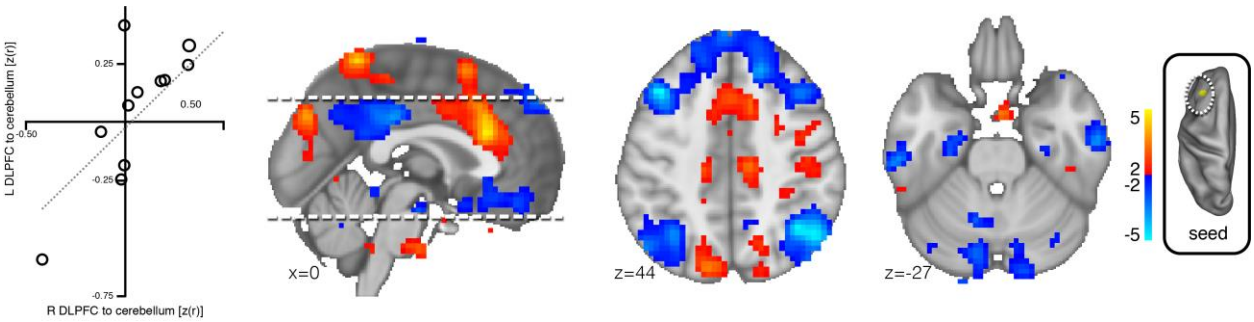

Supplemental Figure 1. Functional connectivity from left dorsolateral prefrontal cortex corresponding to negative symptoms. Right, post-hoc analysis of network discovery cohort, a seed-region was placed in the left dorsolateral prefrontal cortex in all subjects and then this seed-based connectivity map was correlated with symptom severity to identify locations where increasing connectivity to dorsolateral prefrontal cortex corresponds to better symptoms (red) and decreased connectivity corresponds to worse symptoms (blue). Thus, regions in blue correspond to locations where connectivity breakdown with dorsolateral prefrontal cortex corresponds to symptom worsening. Organization of this network is similar to connectivity observed from left dorsolateral prefrontal cortex (see main text figure 1c). Right, correlation of change in connectivity scores in network validation cohort to the cerebellum using either right dorsolateral prefrontal cortex (R DLPFC) or left dorsolateral prefrontal cortex (L DLPFC).

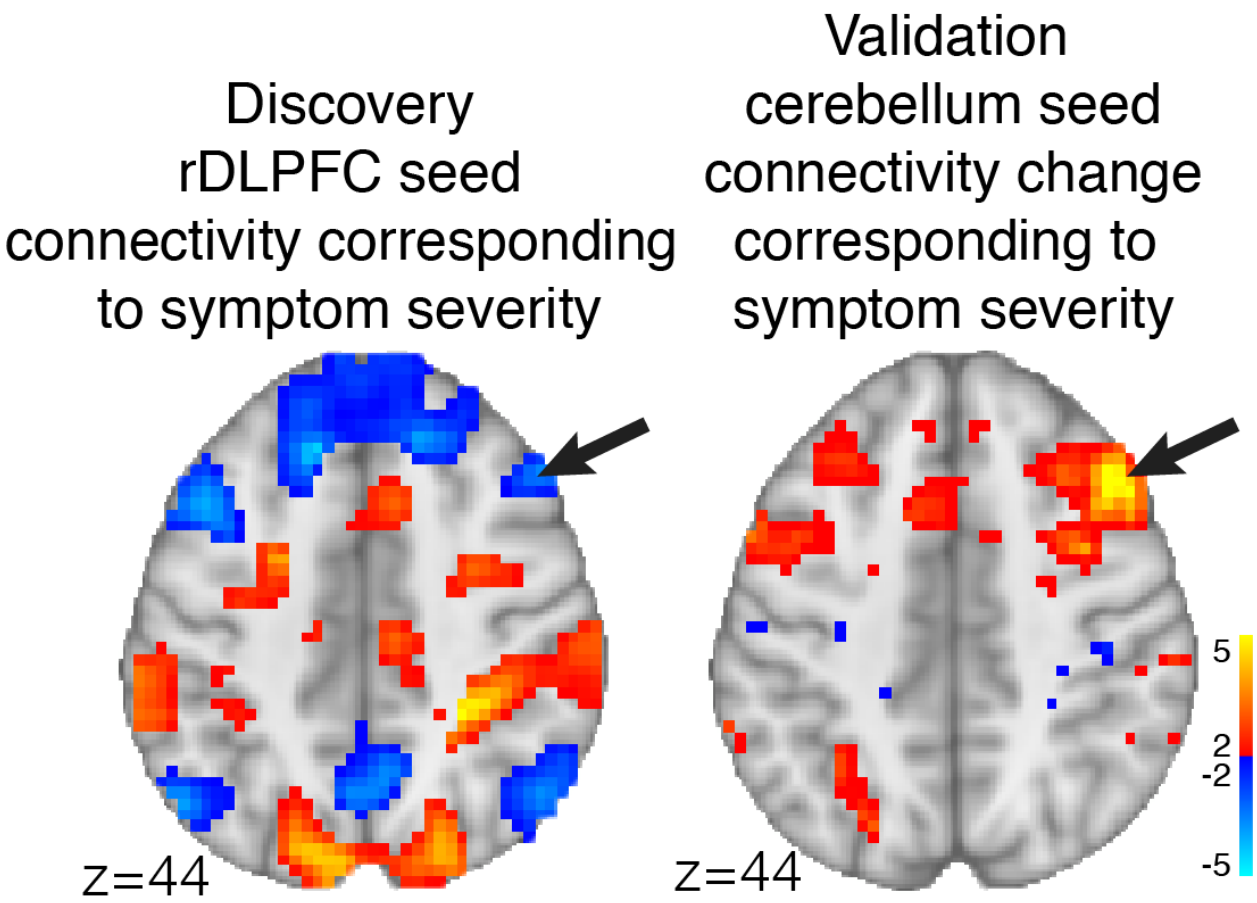

Supplemental Figure 2. Whole brain functional connectivity change in network validation experiment (TMS) from cerebellar seed corresponding to PANSS negative scores. Right, whole brain functional connectivity change from cerebellar seed corresponding to negative symptom reduction (warm colors: increase in connectivity corresponding to symptom reduction; cool colors: decrease in connectivity corresponding to symptom reduction)

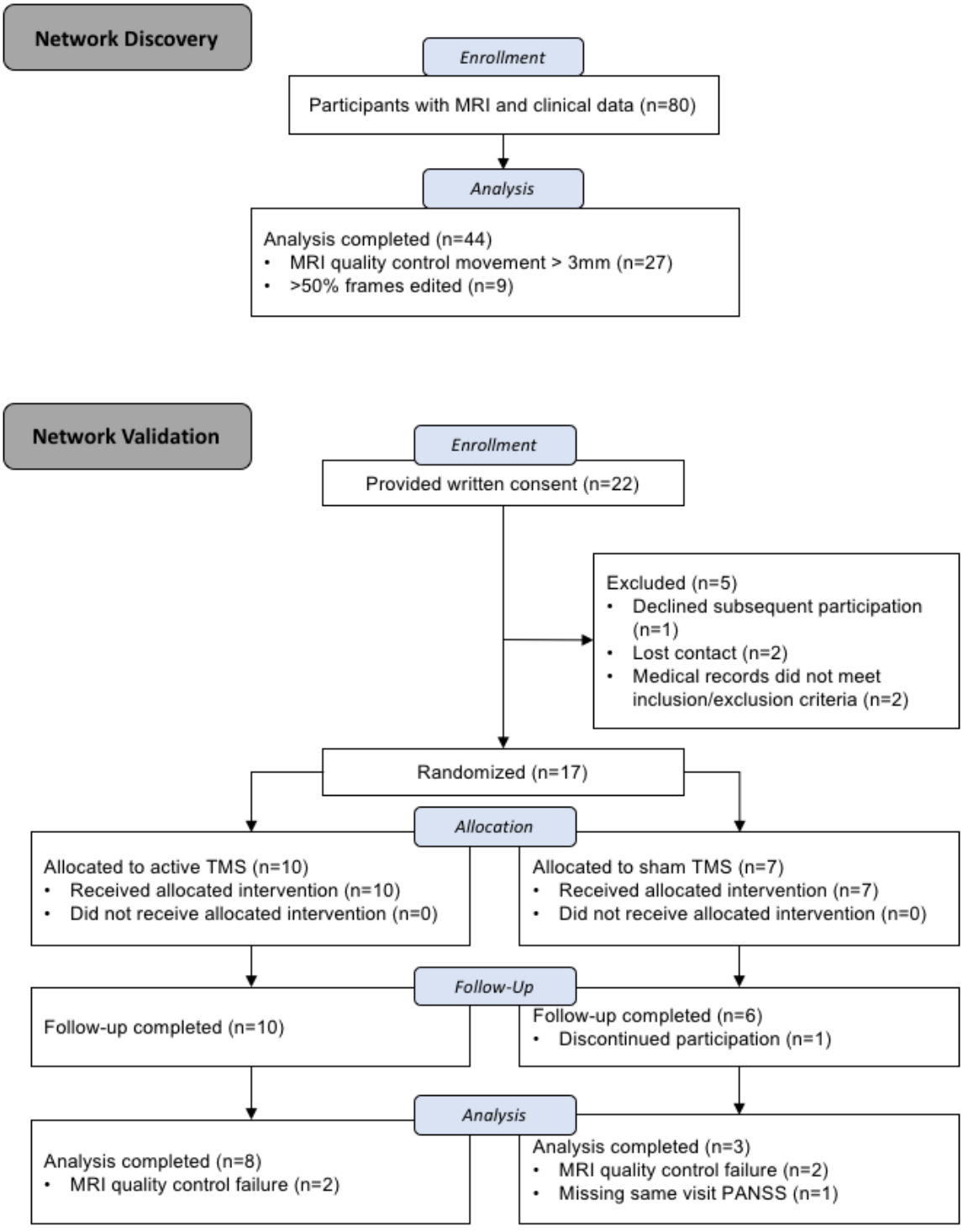

Supplemental Figure 3: CONSORT diagram of participant study flow.

References

1. First MB, New York State Psychiatric Institute. Biometrics Research D: Structured clinical interview for DSM-IV-TR axis I disorders : SCID-I. New York, N.Y., Biometrics Research Dept., New York State Psychiatric Institutute; 2007.
2. Andreasen N: Scale for the Assessment of Positive symptoms (SAPS). Iowa City, University of Iowa; 1984.
3. Andreasen NC. The Scale for the Assessment of Negative Symptoms (SANS): conceptual and theoretical foundations. Br J Psychiatry Suppl. 1989:49-58.
4. Overall JE, Gorham DR. The brief psychiatric rating scale. Psychological Reports. 1962;10:799-812.
5. Montgomery SA, Asberg M. A new depression scale designed to be sensitive to change. Br J Psychiatry. 1979;134:382-389.
6. Yan CG, Wang XD, Zuo XN, Zang YF. DPABI: Data Processing & Analysis for (Resting-State) Brain Imaging. Neuroinformatics. 2016;14:339-351.
7. Power JD, Barnes KA, Snyder AZ, Schlaggar BL, Petersen SE. Spurious but systematic correlations in functional connectivity MRI networks arise from subject motion. Neuroimage. 2012;59:2142-2154.
8. Shehzad Z, Kelly C, Reiss PT, Cameron Craddock R, Emerson JW, McMahon K, Copland DA, Castellanos FX, Milham MP. A multivariate distance-based analytic framework for connectome-wide association studies. Neuroimage. 2014;93 Pt 1:74-94.
9. Sharma A, Wolf DH, Ciric R, Kable JW, Moore TM, Vandekar SN, Katchmar N, Daldal A, Ruparel K, Davatzikos C, Elliott MA, Calkins ME, Shinohara RT, Bassett DS, Satterthwaite TD. Common Dimensional Reward Deficits Across Mood and Psychotic Disorders: A Connectome-Wide Association Study. Am J Psychiatry. 2017:appiajp201616070774.
10. Shanmugan S, Wolf DH, Calkins ME, Moore TM, Ruparel K, Hopson RD, Vandekar SN, Roalf DR, Elliott MA, Jackson C, Gennatas ED, Leibenluft E, Pine DS, Shinohara RT, Hakonarson H, Gur RC, Gur RE, Satterthwaite TD. Common and Dissociable Mechanisms of Executive System Dysfunction Across Psychiatric Disorders in Youth. Am J Psychiatry. 2016;173:517-526.
11. Satterthwaite TD, Vandekar SN, Wolf DH, Bassett DS, Ruparel K, Shehzad Z, Craddock RC, Shinohara RT, Moore TM, Gennatas ED, Jackson C, Roalf DR, Milham MP, Calkins ME, Hakonarson H, Gur RC, Gur RE. Connectome-wide network analysis of youth with Psychosis-Spectrum symptoms. Mol Psychiatry. 2015;20:1508-1515.
12. Cox RW. AFNI: software for analysis and visualization of functional magnetic resonance neuroimages. Comput Biomed Res. 1996;29:162-173.
13. Kay SR, Fiszbein A, Opler LA. The positive and negative syndrome scale (PANSS) for schizophrenia. Schizophrenia bulletin. 1987;13:261-276.
14. Addington D, Addington J, Schissel B. A depression rating scale for schizophrenics. Schizophr Res. 1990;3:247-251.
15. Halko MA, Farzan F, Eldaief MC, Schmahmann JD, Pascual-Leone A. Intermittent theta-burst stimulation of the lateral cerebellum increases functional connectivity of the default network. J Neurosci. 2014;34:12049-12056.

16. Demirtas-Tatlidede A, Freitas C, Cromer JR, Safar L, Ongur D, Stone WS, Seidman LJ, Schmahmann JD, Pascual-Leone A. Safety and proof of principle study of cerebellar vermal theta burst stimulation in refractory schizophrenia. Schizophr Res. 2010;124:91-100.
17. Huang YZ, Edwards MJ, Rounis E, Bhatia KP, Rothwell JC. Theta burst stimulation of the human motor cortex. Neuron. 2005;45:201-206.
18. Kraepelin E, Robertson GM: Dementia praecox and paraphrenia. Edinburgh,, Livingstone; 1919.
19. Tamminga CA, Thaker GK, Buchanan R, Kirkpatrick B, Alphs LD, Chase TN, Carpenter WT. Limbic system abnormalities identified in schizophrenia using positron emission tomography with fluorodeoxyglucose and neocortical alterations with deficit syndrome. Arch Gen Psychiatry. 1992;49:522-530.
20. Weinberger DR, Berman KF, Zec RF. Physiologic dysfunction of dorsolateral prefrontal cortex in schizophrenia. I. Regional cerebral blood flow evidence. Arch Gen Psychiatry. 1986;43:114-124.
21. Heckers S, Goff D, Schacter DL, Savage CR, Fischman AJ, Alpert NM, Rauch SL. Functional imaging of memory retrieval in deficit vs nondeficit schizophrenia. Arch Gen Psychiatry. 1999;56:1117-1123.
22. Schmahmann JD. Dysmetria of thought: clinical consequences of cerebellar dysfunction on cognition and affect. Trends Cogn Sci. 1998;2:362-371.
23. Schmahmann JD. An emerging concept. The cerebellar contribution to higher function. Arch Neurol. 1991;48:1178-1187.
24. Andreasen NC, O'Leary DS, Cizadlo T, Arndt S, Rezai K, Ponto LL, Watkins GL, Hichwa RD. Schizophrenia and cognitive dysmetria: a positron-emission tomography study of dysfunctional prefrontal-thalamic-cerebellar circuitry. Proc Natl Acad Sci U S A. 1996;93:9985-9990.
25. Picard H, Amado I, Mouchet-Mages S, Olie JP, Krebs MO. The role of the cerebellum in schizophrenia: an update of clinical, cognitive, and functional evidences. Schizophrenia bulletin. 2008;34:155-172.
26. Andreasen NC, Pierson R. The role of the cerebellum in schizophrenia. Biol Psychiatry. 2008;64:81-88.
27. Kim DJ, Kent JS, Bolbecker AR, Sporns O, Cheng H, Newman SD, Puce A, O'Donnell BF, Hetrick WP. Disrupted modular architecture of cerebellum in schizophrenia: a graph theoretic analysis. Schizophrenia bulletin. 2014;40:1216-1226.
28. Kahn RS, Sommer IE, Murray RM, Meyer-Lindenberg A, Weinberger DR, Cannon TD, O'Donovan M, Correll CU, Kane JM, van Os J, Insel TR. Schizophrenia. Nat Rev Dis Primers. 2015;1:15067.
29. Buckner RL, Krienen FM, Castellanos A, Diaz JC, Yeo BT. The organization of the human cerebellum estimated by intrinsic functional connectivity. J Neurophysiol. 2011;106:2322-2345.